

# Automatic Lung Segmentation in MDCT Images

Oliver Weinheimer<sup>1</sup>, Tobias Achenbach<sup>2</sup>, Claus Peter Heussel<sup>3</sup>, and  
Christoph Düber<sup>1</sup>

<sup>1</sup> Department of Diagnostic and Interventional Radiology, Johannes Gutenberg University of Mainz, Germany, [weinheim@radiologie.klinik.uni-mainz.de](mailto:weinheim@radiologie.klinik.uni-mainz.de)

<sup>2</sup> Diagnostische und Interventionelle Radiologie, St. Vinzenz-Hospital Köln

<sup>3</sup> Diagnostische und Interventionelle Radiologie, Thoraxklinik Heidelberg

**Abstract.** A fast and reliable segmentation of the lung tissues is of fundamental importance for many clinical applications like emphysema quantification or lung nodule detection. In this paper we present a method for fully automated extraction of the lungs from volumetric computed tomography (CT) images. The method consists of 6 main steps: (1) Segmentation of tracheobronchial tree. (2) Landmark determination in left and right lung. (3) Threshold based region growing. (4) Filling of holes in axial slices. (5) Lung separation if necessary. (6) Morphologic closing with a spherical structural element.

An evaluation on 55 clinical datasets (LOLA11-datasets) shows that the segmentations of our method achieves a good average volumetric overlap (97%) against manually generated reference segmentations.

## 1 Introduction

X-ray computed tomography (CT) is currently the method of choice for noninvasive and sensitive imaging of pathologic changes of lung morphology. Development of multi-detector X-ray CT (MDCT) combines the advantages of the high-resolution CT (HRCT) and spiral CT and allows visualization of the lungs and the bronchial tree up to the subsegmental level. The technology of MDCT provides volume data sets with approximately isotropic resolution. Typical resolution values for thin-section MDCT datasets of the thorax in the clinical routine are about 0.6 mm for in-slice spacing (pixel spacing) and between 0.6 mm and 1.25 mm for slice thickness and slice spacing. Most of the time the field of view (FOV) of the scans is chosen so, that the entire body is shown in the reconstructed axial CT image, see Fig. 1(a)-(d). As a consequence, the in-slice spacing may vary slightly for different patients depending on the chosen FOV.

Depending on anatomical variations and pathological changes lung segmentation can be demanding. Although pathological changes (geographic ground-glass opacity) are visible in Fig. 1(a), it can be termed as a 'usual' lung CT image, in the sense that typical characteristics can be seen: both lungs are well separated and are clearly to see as dark, hypodense regions, the contrast between lung tissue and surrounding anatomy is high. Traditionally CT images are displayed with gray values representing the CT numbers, calculated in the image

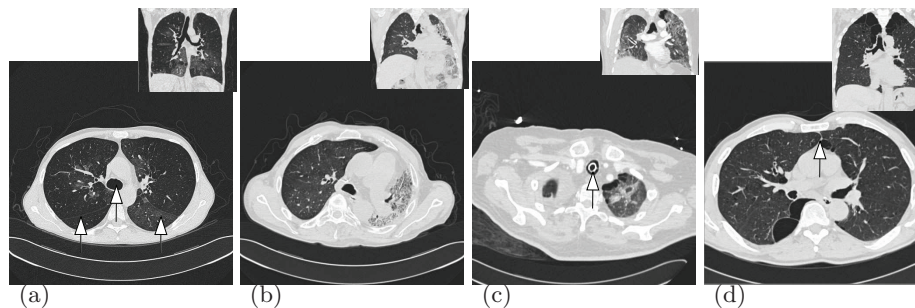


**Fig. 1.** Axial lung CT images of four different patients plus small coronal overview images for every patient. These datasets are not part of the LOLA11 datasets. (a) Case 1 (‘usual case’) at the level of the carina: lungs are well separated, high contrast between lung tissue and surrounding anatomy. The arrows point to (from left to right): right lung, trachea, left lung. (scanner: Siemens Sensation 16, kernel: B70s, pixel spacing: 0.74 mm, slice thickness: 1.00 mm, spacing between slices: 1.00 mm, Exposure: 63 mAs, x-ray tube current: 120 kVp, level/window: [-500/1500]). (b) Case 2 at level of the carina: fibrotic transformations of the lung parenchyma with consecutive shrinkage of the left hemithorax, condition after transplantation of the right lung. (Siemens Volume Zoom, B40f, 0.74 mm, 1.25 mm, 1.00 mm, 70 mAs, 280 kVp, [-500/1500]). (c) Case 3 at top-level of right lung: patient with tracheal intubation, tube inside trachea marked with an arrow. Fibrotic transformations in both lungs. (Siemens Volume Zoom, B40f, 0.74 mm, 1.25 mm, 1.00 mm, 120 kVp, [-500/1500]). (d) Case 4 at lower level of the lungs: severe emphysema patient, lungs are connected (arrow), this is more often the case for emphysema patients. (Siemens Volume Zoom, B30f, 0.63 mm, 1.25 mm, 1.00 mm, 100 mAs, 120 kVp, [-500/1500]).

reconstruction process. White represents generally dense material and black low density material. Roughly speaking, the dimensionless defined CT number, expressed in Hounsfield Units [HU], is proportional to the average relative linear attenuation in a voxel, the CT number of water is defined as 0 HU and air is -1000 HU [1, pg. 32]. Lung CT images of patients with no or mild pathologic changes in the lung tissue will look, in broad outlines, similar to the CT shown in Fig. 1(a). Fig. 1(b)-(d) are more specific or ‘unusual’ images. In Fig. 1(b) the left lung volume is reduced due to fibrotic transformations of the lung parenchyma with consecutive shrinkage of the left hemithorax. This dataset was obtained after transplantation of the right lung. Huge parts of the left lung show less or no contrast to the surrounding anatomy. This scan was obtained at expiration, the other 3 scans in Fig. 1 were obtained at inspiration. The trachea of the patient in Fig. 1(c) was intubated, a white high contrasted ring is displayed in the trachea. Fig. 1(d) shows a CT of an emphysema patient, the right and left lungs are connected. These are just four examples showing how much thoracic CT images can differ. On the one hand clinical applications should be able to handle severe pathologic lung CT images like displayed in Fig. 1(b)-(d), e. g. for longitudinal studies. On the other hand they should also be sensitive enough to find pathologic lung changes in an early state because a precocious diagnosis is the best way

to ensure the success of a treatment. A fast and reliable segmentation of the lung tissues and of the airway tree is of fundamental importance for different clinical applications like a noninvasive 3D measurement and quantification of airway geometry [2, 3], computer-assisted bronchoscopy [4], emphysema quantification [5] or lung nodule detection [6]. MDCT chest scans have become indispensable in thoracic radiology, but have also substantially increased the data load for radiologists. In the recent years low dose CT scans and ultra low dose scans are increasingly utilized in lung screening studies. Aim of study [7] was to define the threshold where reduced dose has significant impact on quantitative emphysema parameters. Different mAs levels were simulated (10 – 100 mAs, 10 mAs increments) and it is shown that the mean lung density (MLD) was equal for 20 – 100 mAs, the variation of the emphysema index (EI, relative lung area below a predefined HU threshold) was below 2 % down to 30 mAs (but strictly increasing from 0.12 for 100 mAs to 3.44 for 10 mAs). The same group shows in [8] via visual ranking of different simulated mAs levels (10 – 100 mAs) of chest images that imaging doses could be lowered down to 60 mAs without a diagnostically relevant increase in noise impairing image quality. Lowering the radiation exposure is a benefit of patients if it is not accompanied with a diagnostically relevant increase in noise impairing image quality. Although these studies show that lowering the radiation exposure is reasonable it is also clear that it increases the amount of noise in the CT images, hence it increases the demands on lung and airway extraction methods. Automating the analysis of such data is, therefore, a necessity and this has created a rapidly developing research area in medical imaging. So far, there have been no perfect extraction techniques for the lungs and tracheobronchial tree.

The following section is structured as follows: Firstly, we will give a short review of existing methods described in literature for lung segmentation. Secondly, the methods implemented in our in-house software *yacta* ('yet another CT analyzer') are described. The methods used in *yacta* are based on the methods first introduced in [9]. The software was improved over time while using it for many studies, see e.g. [10, 11, 7, 12, 2, 13, 14, 5, 15]. *yacta* works fully automated - it is possible to send DICOM images from an arbitrary DICOM Viewer to it or to use the software via a batch-file.

## 2 Review of existing methods

We start with the work presented in [16] – an automated, knowledge-based method for segmenting chest CT datasets. Anatomical knowledge like expected volume, shape, relative position and CT number range of organs are used for guidance of the segmentation process. Lung segmentation is done by X-ray attenuation thresholding between -1024 and -500 HU. If the two lung fields are connected to one region, as in the case illustrated in Fig. 1(d), the anterior junction line is followed by calculation of a maximum cost path. The rationale for using a maximum cost path algorithm is that the soft tissue of the anterior junction line separating the right and left lungs can be very thin, but the junction

line has a slightly higher gray-level than the lungs, and forms a continuous line in each axial slice of the connecting region, even if the CT numbers on the junction line are  $\leq -500$  HU. As cost of a pixel its CT number is used. Segmentation was performed on data from two healthy subjects and five patients with emphysema and the accuracy of the segmentations was subjectively assessed by two radiologists. Later in [17] the lung segmentation was applied to scans of 49 patients containing 1313 axial images. Manual editing was required to correct 183 (13.94%) of the images. The segmentation results were inspected by an expert observer and the sensitivity, specificity, and accuracy were greater than 98.55% in classifying pixels as lung or non-lung.

In [18] a fully automatic method for identifying the lungs in CT images is described. The method has three main steps. First, the lung region is extracted from the CT images by gray-level thresholding. The histogram of the scan is assumed to be bimodal and iteratively the optimal gray value threshold separating the two distributions is found. The background air is eliminated by deleting regions that are connected to the border of the image. Small, disconnected regions are discarded if the region volume is too small. The lungs are identified as the two largest components in the volume, with the additional constraint that each component must be larger than a predetermined minimum volume (1% of the total image voxel count). Then, the trachea and main bronchi are removed. Sometimes only one connected component is found. The left and right lungs are then separated by detecting the anterior and posterior junctions. To separate the connected lungs in this case, dynamic programming in axial slices is applied to find the maximum cost path using a technique similar to that employed in [16]. Finally, the lung boundary is optionally smoothed with a sequence of morphological operations. Eight normal subject were scanned three times at approximately two week intervals at full inspiration using a lung volume monitoring system. For each point  $a$  of the segmented lung borders  $S_{\text{seg}}$ , the minimum distance  $d_{\text{min}}(a, S_{\text{man}}) = \min_{b \in S_{\text{man}}} (\|a, b\|)$  to the manually defined lung border  $S_{\text{man}}$  in the same axial image was determined. Then the mean, root mean square and maximum over all these distances were computed:

$$d_{\text{mean}}(S_{\text{seg}}, S_{\text{man}}) = \frac{\sum_{a \in S_{\text{seg}}} d_{\text{min}}(a, S_{\text{man}})}{|S_{\text{seg}}|} \quad (1)$$

$$d_{\text{rms}}(S_{\text{seg}}, S_{\text{man}}) = \sqrt{\frac{\sum_{a \in S_{\text{seg}}} d_{\text{min}}(a, S_{\text{man}})^2}{|S_{\text{seg}}|}} \quad (2)$$

$$d_{\text{max}}(S_{\text{seg}}, S_{\text{man}}) = \max_{a \in S_{\text{seg}}} d_{\text{min}}(a, S_{\text{man}}) \quad (3)$$

$d_{\text{mean}}$  between the computer-defined borders and manually defined borders was about 0.48 pixels. Lung volume calculations showed that the results are reproducible over the 3 different points in time, small variations in computed volumes are primarily due to differences in the level of lung inflation.

Methods similar to those presented by [16] and [18], i.e. methods based on thresholding, region growing, morphological operations and an additional step for lung separation, are denoted as *conventional methods* in the following.

In [19] the authors propose a segmentation-by-registration scheme in which a scan with normal lungs is elastically registered to a scan containing pathology. For the elastic registrations they used the VTK CISG Registration Toolkit. In order to correct the drawback of the segmentation-by-registration scheme, namely that it cannot accommodate small scale differences between normal lung shapes, they use a probabilistic atlas segmentation from several normal subjects and a voxel classification procedure to refine the segmentation-by-registration result. The found deformations are applied separately to the left and right lung, region overlap is avoided. The overall method is very time consuming (several hours for one scan). The Performance of the segmentation-by-registration scheme was compared to three other algorithms: an automatic conventional method based on the procedure of [18], a interactive region growing method and a voxel classification algorithm. 10 Scans were used for comparison. The evaluation was performed against reference segmentations using the volumetric overlap, the symmetric Hausdorff distance and the mean absolute surface distance. The volumetric overlap of the segmented volume  $V_1$  and the reference volume  $V_2$  is defined as:

$$O(V_1, V_2) = \frac{\|V_1 \cap V_2\|}{\|V_1 \cup V_2\|}, \quad (4)$$

the volume of their intersection divided by the volume of their union.  $d_{\max}(S_{\text{seg}}, S_{\text{man}})$  in equation (3) is also called directed Hausdorff distance – it is an asymmetric distance measure. The symmetric Hausdorff distance  $d_H(S_{\text{seg}}, S_{\text{man}})$  is an extension the directed one:

$$d_H(S_{\text{seg}}, S_{\text{man}}) = \max(d_{\max}(S_{\text{seg}}, S_{\text{man}}), d_{\max}(S_{\text{man}}, S_{\text{seg}})), \quad (5)$$

with  $d_H(S_{\text{seg}}, S_{\text{man}}) = d_H(S_{\text{man}}, S_{\text{seg}})$ . The mean absolute surface distance is defined as:

$$d_{\text{masd}} = \frac{d_{\text{mean}}(S_{\text{seg}}, S_{\text{man}}) + d_{\text{mean}}(S_{\text{man}}, S_{\text{seg}})}{2}. \quad (6)$$

The automatic conventional method was unable to adequately segment the pathological test scans. In segmenting high density tissues (pathologic tissue) both voxel classification and (refined) segmentation-by-registration outperformed the manually aided region growing method, but it is also noted that the average results mostly show no significant differences between those three methods.

[6] proposed a new stochastic framework for accurate lung segmentation. They describe low dose CT scans and desired maps of regions (lung and other chest tissues) by a joint Markov-Gibbs random field model (MGRF) of independent image signals and interdependent region labels but focus on most accurate model identification. To better specify region borders, each empirical distribution of image gray values is approximated by a linear combination of discrete Gaussians (LCDG) with positive and negative components. They modified a conventional Expectation-Maximization (EM) algorithm to deal with the LCDG and

develop a sequential EM-based technique to get an initial LCDG-approximation for the modified EM algorithm. The initial segmentation based on the LCDG-models is then iteratively refined using a MGRF model with analytically estimated potentials. Experiments on 10 real data sets, each consisting of 182 slices, confirm high accuracy of the proposed approach. It is not mentioned how well the methodology works with severely pathological images. Also lung separation is not a topic in the article.

[20] presented a lung segmentation algorithm called Adaptive Border Marching (ABM). The primary emphasis of the method is to include juxta-pleural nodules in the lung segmentation result. The preprocessing stage contains three steps: Firstly a Gaussian smoothing of the CT dataset is done. Secondly the images are thresholded with -500 HU as threshold and thirdly the non-lung region was flood-filled. After preprocessing the lung borders were tracked. Then defects in the lung borders caused by juxta-pleural nodules, to note as local concavities, were corrected, while minimizing undersegmentation and oversegmentation relative to the true lung border. The method was tested against 20 datasets containing 67 nodules. All nodules were correctly re-included. Lung separation is not treated in the article.

The basic idea behind the method suggested by [21] is that one would expect the curvature of the ribs and the curvature of the lung boundary around the ribs to be very close. Inspired by this, firstly the ribs are segmented by applying a threshold algorithm with threshold of 200 HU, followed by different morphologic operations. Morphological thinning constitutes the final step, then the curve of the ribs is represented using polynomial interpolation. The lung segmentation scheme uses a multi-threshold iterative approach. The threshold value is dynamically changed in increments of 5 HU until the curvature of the ribs and the curvature of the lung boundary are closely matched. The lung boundary is matched in such a way that there is minimal deviation (mean squared difference) from the polynomial representation of the ribs. Performance of this technique was compared with conventional fixed threshold lung segmentation techniques on 19 subjects using a volumetric overlap fraction measure. The evaluation was performed against reference segmentations using the volumetric overlap of the segmented volume  $V_1$  and the reference volume  $V_2$  as measure, see equation (4). The technique outperforms the conventional approach in the presence of abnormal regions from subjects having asthma, emphysema, or scleroderma. However, by lowering the threshold, other non-lung regions not bordering the ribs are included into the segmentation result. The task of lung separation is not treated.

The method proposed in [22] is meant to be used as preprocessing step in the computer-assisted detection (CAD) system for malignant lung nodule detection. The algorithm was initially developed and tested on a dataset of 130 CT scans and then applied on another 139 scans, giving very satisfactory results – the lung contour was adequately located in 96% of the CT scans (volumetric overlap was used as measure, just a subset of 36 randomly chosen datasets were manually segmented as ground truth). The method consists of several steps. At first an appropriate gray-value threshold for the segmentation of the respiratory appara-

tus is found by histogram analysis. Then the trachea, the bronchi and the lungs are segmented by 3D region growing using this threshold. External airways are removed from this segmentation. If the lungs are connected a separation surface between the lungs is constructed and the lungs are divided in left and right. Finally a morphologic closing with a fixed size spherical structural element is performed, the chosen diameter was 30 mm.

[23] presented a hybrid lung segmentation method. First a method similar to the the procedure introduced by [18] is applied to a dataset. Four factors were used for the automatic error detection: (1) volume of the left lung, (2) volume of the right lung, (3) ratio between the volumes of left and right lung and (4) shape consistency of the lung border. For the first three components, minimum and maximum values were observed from 320 training datasets. The fourth component is based on the rational that the shape of the costal lung surface is convex. The convexity of the segmented costal lung surface is compared to the convex hull of this costal lung surface. Crucial differences between the costal lung surface and the convex hull of it are likely to indicate errors in the segmentation. If a lung segmentation fails on one of the four tests it is marked as possibly erroneous. The scans that are likely to contain errors are then segmented by a more sophisticated algorithm, based on multiatlas segmentation. This algorithm is likely to perform better for cases containing abnormal pathology but is considerably slower than the conventional algorithm. In a quantitative evaluation on a database of 150 scans from different sources, the hybrid method is shown to perform substantially better than a conventional approach. By applying only the conventional method 55 s per scan were needed for the segmentation of the 150 scans in the database, the average segmentation time only with the multiatlas segmentation was 120 min per scan. Applying the hybrid methods leads to 22 possibly erroneous scans, detected by the error detection, those 22 scans were additionally segmented with the multiatlas method. The average segmentation time was 18.6 min per scan for the 150 scans in the database. The conventional method failed to found the lungs in 3 cases, marked a too low lung volume in 6 cases and a shape error was detected at the costal surface of the lungs. An interesting fact reported in this article is that the conventional method follows the lung border more precise than both the multiatlas method and the manual tracing in the 128 cases in which no error occurred.

### 3 Automatic Lung Segmentation via *yacta*

The article [19] closes with the remark: “Segmentation in presence of pathology continues to be one of the biggest challenges in medical image analysis . . . but as of yet, performance of a human observer remains unequaled by that of any of the automated methods.” That is definitely a truth – still today, 6 years later. Furthermore in this article is shown that the results of the interactive conventional method mostly show no significant differences to the results of the compared segmentation-by-registration scheme and voxel classification method. This is caused by the fact that not segmented lung regions (by the interactive

conventional method) are mostly just small parts of the lung. In [23] was reported that the conventional method follows the lung border more precise than the proposed multiatlas method and the manual tracing when no abnormalities are present. The conventional method leads to erroneous lung segmentation when abnormalities are present, but there are also suggestions for improvement for the conventional method. In practice, there is a trade-off between required computation time and quality of the segmentation results. The results should be as precise as possible and available in as little time as possible. Additionally, methods usable in the clinical routine also need to have about a high degree of robustness. Against this background, advanced conventional methods are a suitable solution for lung segmentation. Conventional methods are very fast, however, it is important to use advanced methods for landmark determination, lung separation, and for the inclusion of high density abnormalities and vessels.

The algorithm currently used in *yacta* can be classified as an advanced conventional method and consists of following steps:

1. Segmentation of tracheobronchial tree.
2. Landmark determination in left and right lung.
3. Threshold based region growing.
4. Filling of holes in axial slices.
5. Lung separation if necessary.
6. Morphologic closing operation with a spherical structural element.

New releases of *yacta* are tested on a database containing currently more than 150 scans from different sources. This gives the possibility to develop the software step by step, without losing quality achieved already. Step 1 is mostly addressed in article [24]. Of course, any other algorithm for segmentation of the bronchial tree can be used at this point. In step 2 first the main bifurcation of the trachea is determined (landmark “carina”). Then the whole body is labeled on the slice containing the landmark “carina”. The left respectively right lung are searched as low density structures inside the body not marked as bronchial tree. If the left or right lung are not found on this slice, adjacent slices are examined. The method stops if the slice containing the landmark “trachea” is reached in cranial direction. If the search fails in cranial direction the same number of slices are examined in caudal direction. In step 3 two region growing processes with default threshold -500 HU are started, one in the left and one in the right lung. Optionally optimal thresholding ([25, pg. 742-774]) can be applied – therefore a set of 10 slices around the level of the landmark “carina” is used. Extra-corporeal voxels are not taken into account when calculating the optimal threshold value. Exclusion of the extra-corporeal air generally leads to a higher optimal threshold and to better segmentation results. A 2D hole filling algorithm is applied in step 4 to include high density structures. We use a 2D version because the results are, in our opinion, more like a physician would mark the lung - mostly all high density structures surrounded by low density lung parenchyma are included to the segmentation. Step 5 is an optional step. It is performed if only one connected component is found by the two region growing processes of step 3. In these cases, a fast marching minimal path extraction method is applied on the



axial images. The method is an adaption of the algorithm suggested in [26, 27]. Step 6 is performed in order to include sub-pleural abnormalities and concavities to the lung. Therefore the lung segmentation is dilated by a one voxel thick layer and then optionally a morphological closing with an spherical kernel with diameter 10 mm is applied.

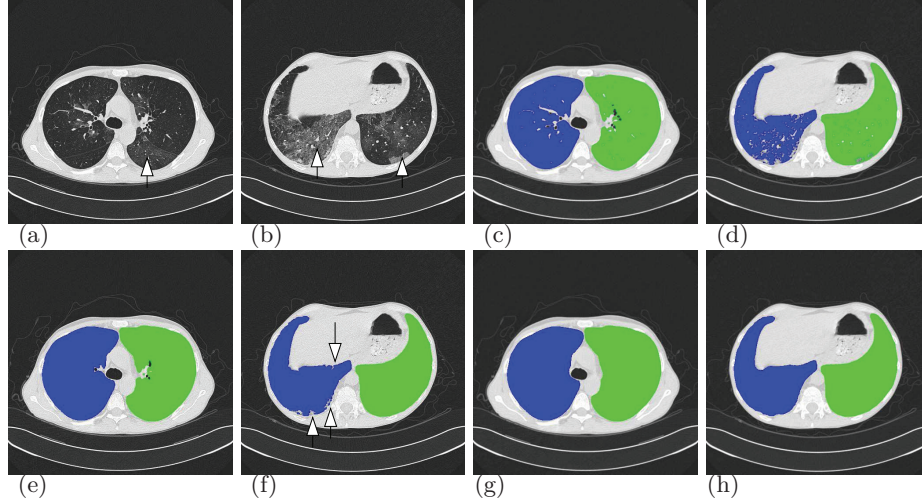


**Fig. 2.** Case 1. (a)(b) The arrows point to slight pathological changes in the lungs (ground-glass opacity). (c)(d) Segmentation result after region growing step with default threshold of -500 HU. The two region growing processes result in two distinct regions. (e)(f) Result after filling step. The arrows point to not segmented regions belonging to the right lung. (g)(h) Result after morphologic closing. Pleural structures are correctly included.

We now consider how the automatic methodology implemented in *yacta* deals with the four cases presented in Fig. 1. Fig. 2 shows the segmentation results for case 1, where only minor pathological changes are visible. The arrows in Fig. 2(a)(b) point to regions with ground-glass opacity. After step 3 the lungs are separated but parts of the lungs with higher density are omitted, see Fig. 2(c)(d). These parts are partly added to the segmentation after step 4 displayed in Fig. 2(e)(f). Step 5 was not necessary and step 6 added the pleural abnormalities shown in Fig. 2(f) and additionally airways and vessels near the lung border, compare Fig. 2(e) with Fig. 2(g), to the lung segmentation. We thus obtained a completely satisfactory segmentation result.

Fig. 3(a)(c) shows the severe pathologic changes of the lung in case 2. In Fig. 3(b)(d) the automatic segmentation results after step 6 are displayed. Just the upper part of the left lung is segmented, this is caused by the fact that the landmark in the left lung is found in the upper half of the lung. Changing the default threshold used in step 3 from -500 HU to -385 HU by optimal thresholding

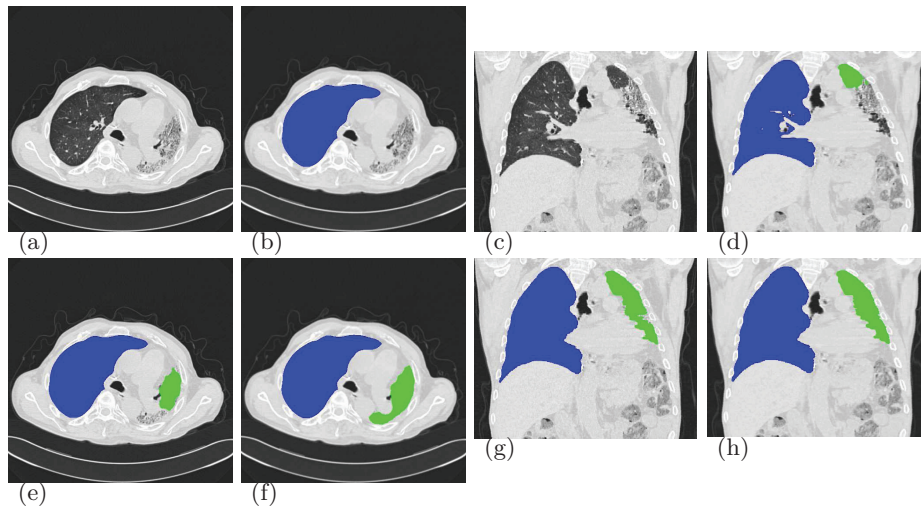


**Fig. 3.** Case 2. (a)(c) The thorax CT shows fibrotic transformations of the lung parenchyma with consecutive shrinkage of the left hemithorax (condition after lung transplantation on the right lung). (b)(d) Segmentation results after default automatic segmentation by *yacta* with threshold -500 HU. (e)(g) Segmentation results using an calculated optimal threshold of -385 HU in step 3. (f)(h) Results with manually selected threshold of -200 HU.

results in obviously better segmentations displayed in Fig. 3(e)(g) but parts of the left lung are still omitted. Manually changing the threshold to -200 HU leads to a satisfactory segmentation results.

Fig. 4 and Fig. 5 shows the results for case 3 and case 4. Using a higher threshold of -200 HU would again lead to more satisfactory results for case 3. Case 4 is an example where only one connected component is found in step 3 - the lungs are well separated by the minimal path finding algorithm applied in step 5.

Note, the datasets displayed in this and the previous section are not part of the LOLA11 datasets.

## 4 Results and Discussion

The images used in this challenge were volumetric chest CT scans acquired at different sites using several different scanners, scanning protocols, and reconstruction parameters.

The automatic lung segmentation methodology implemented in *yacta* was applied to all 55 LOLA11-datasets twice. Optimal Thresholding in step 3 was used by default, but the optionally morphological closing in step 6 was once applied, once not. Table 1 lists the results of the method without morphological closing and Table 2 lists the results with morphological closing (spherical kernel 10 mm). As measure the volumetric overlap fraction was used, which is

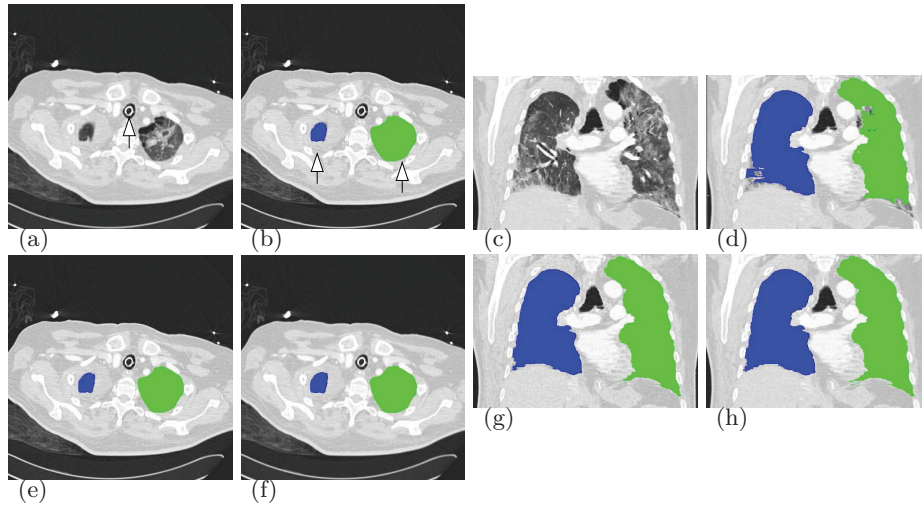


**Fig. 4.** Case 3. (a)(c) Patient with tracheal intubation and fibrotic transformations in both lungs. (b)(d) Segmentation results after default automatic segmentation by *yacta* with threshold -500 HU. (e)(g) Segmentation result with threshold -351 HU obtained by optimal thresholding. (f)(h) Results with manually selected threshold of -200 HU.

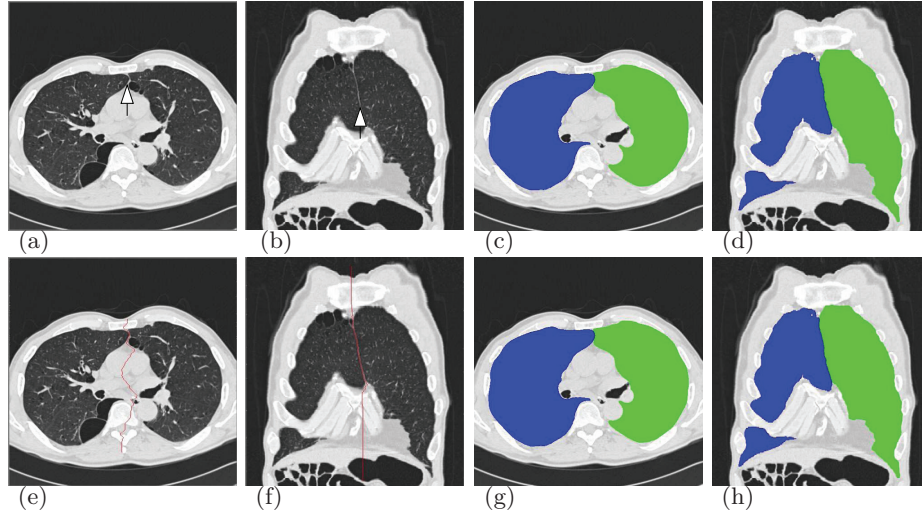


**Fig. 5.** Case 4. (a)(b) Severe emphysema patient, lungs are connected (arrows). (e)(f) Separation of the lungs via minimal path calculation in step 5, path displayed as red line. (c)(d) Result after morphologic closing and default thresholding (-500 HU) in step 3. (g)(h) Result after morphologic closing and optimal thresholding (-382 HU) in step 3.

a measure that compares the relative volumetric overlap of two binary segmentations, see equation (4). The more equal two segmentations are, the closer the volumetric overlap fraction is to one. The segmentation results with morphological closing (score: 0.970) are with respect to this measure slightly better as the results without closing (score: 0.964). The average runtime on a PC (Intel Xeon CPU, 2.83 GHz, 4GB RAM) per case was 7.3 minutes without morphological closing and 11.4 minutes with morphological closing. For details on the set-up of the study, collection of data and evaluation of segmentations see <http://www.lola11.com/>.

**Table 1.** Results of lung segmentation for the 55 scans in LOLA11 - without morphological closing.

	mean	SD	min	Q1	median	Q3	max
left lung	0.965	0.0986	0.265	0.974	0.984	0.991	0.995
right lung	0.963	0.134	0	0.982	0.986	0.991	0.995
score	0.964						

**Table 2.** Results of lung segmentation for the 55 scans in LOLA11 - with morphological closing.

	mean	SD	min	Q1	median	Q3	max
left lung	0.971	0.0925	0.309	0.982	0.988	0.992	0.997
right lung	0.969	0.134	0	0.986	0.99	0.993	0.998
score	0.970						

Our implementation can be classified as advanced conventional method. The good score achieved with this method shows that it is a suitable solution for lung segmentation. Nevertheless there are still problems to solve and ideas to improve the method, e. g.

- Using a higher HU threshold for the threshold based segmentation in step 3 can lead to a better segmentation, see Fig. 3 and Fig. 4.
- The minimal path algorithm is implemented in 2D, working on axial slices. This should be a real 3D method.
- Integration of a robust lobe segmentation.
- Faster runtime.
- Better airway tracer.

In this paper we presented a method for fully automated segmentation of the lungs from CT Scans. Our method worked well on the challenging datasets of LOLA11, nevertheless we have gathered valuable information for our future

work. Generating a common database covering a wide range of possible CT scans is an important step for improving and comparing different lung segmentation methods.

This work was supported by DFG Grant WE 4691/2-1.

## References

1. Herman, G.T.: Fundamentals of computerized tomography: Image reconstruction from projections. 2. ed. edn. Advances in pattern recognition. Springer-Verlag and Springer, London (2009)
2. Achenbach, T., Weinheimer, O., Biedermann, A., Schmitt, S., Freudenstein, D., Gouthma, E., Kunz, R.P., Buhl, R., Dueber, C., Heußel, C.P.: MDCT Assessment of Airway Wall Thickness in COPD Patients Using a New Method: Correlations with Pulmonary Function Tests. *European Radiology* **18** (2008) 2731–2738
3. Saba, O.I., Hoffman, E.A., Reinhardt, J.M.: Maximizing Quantitative Accuracy of Lung Airway Lumen and Wall Measures Obtained from X-Ray CT Imaging. *Journal of Applied Physiology* **95** (2003) 1063–1075
4. Kiraly, A.P., Helferty, J.P., Hoffman, E.A., McLennan, G., Higgins, W.E.: Three-Dimensional Path Planning for Virtual Bronchoscopy. *IEEE Trans. Med. Imaging* **23**(9) (2004) 1365–1379
5. Heußel, C.P., Herth, F., Kappes, J., Hantusch, R., Hartlieb, S., Weinheimer, O., Kauczor, H.U., Eberhardt, R.: Fully-automatic quantitative assessment of emphysema in computed tomography – comparison with pulmonary function testing and normal values. *European Radiology* **19**(10) (2009) 2391–2402
6. El-Baz, A., Gimel'farb, G.L., Falk, Robert, Holland, T., Shaffer, T.: A new stochastic framework for accurate lung segmentation. In Dimitris N. Metaxas, Leon Axel and Gabor Fichtinger and Gábor Székely, Metaxas, D., Axel, L., Fichtinger, G., Székely, G., eds.: *Medical Image Computing and Computer-Assisted Intervention - MICCAI 2008*, 11th International Conference, New York, NY, USA, September 6–10, 2008, Proceedings, Part I. Volume 5241 of *Lecture Notes in Computer Science*. Springer (2008) 322–330
7. Zaporozhan, J., Ley, S., Weinheimer, O., Eberhardt, R., Tsakiris, I., Noshi, Y., Herth, F., Kauczor, H.U.: Multi-detector ct of the chest: Influence of dose onto quantitative evaluation of severe emphysema a simulation study. *Journal of Computer Assisted Tomography* **30**(3) (2006) 460–468
8. Ley-Zaporozhan, J., Ley, S., Krummenauer, F., Ohno, Y., Hatabu, H., Kauczor, H.U.: Low dose multi-detector ct of the chest (ilead study): Visual ranking of different simulated mas levels. *European Journal of Radiology* **73**(2) (2010) 428–433
9. Weinheimer, O., Achenbach, T., Buschsieweke, C., Heußel, C.P., Uthmann, T., Kauczor, H.U.: Quantification and Characterization of Pulmonary Emphysema in Multislice-CT: A Fully Automated Approach. In Petra Perner, Rüdiger W. Brause and Hermann-Georg Holzhütter, eds.: *Medical Data Analysis*, 4th International Symposium, ISMDA 2003, Berlin, Germany, October 9–10, 2003, Proceedings. Volume 2868 of *Lecture Notes in Computer Science*. Springer (2003)
10. Achenbach, T., Weinheimer, O., Buschsieweke, C., Heußel, C.P., Thelen, M., Kauczor, H.U.: Fully automatic detection and quantification of emphysema on thin section md-ct of the chest by a new and dedicated software. *RöFo: Fortschritte auf dem Gebiet der Röntgenstrahlen und der bildgebenden Verfahren* **176** (2004) 1409–1415

14 Weinheimer et al.

11. Zaporozhan, J., Ley, S., Eberhardt, R., Weinheimer, O., Iliyushenko, S., Herth, F., Kauczor, H.U.: Paired inspiratory/expiratory volumetric thin-slice ct scan for emphysema analysis: comparison of different quantitative evaluations and pulmonary function test. *Chest* **128** (2005) 3212–3220
12. Ley-Zaporozhan, J., Ley, S., Eberhardt, R., Weinheimer, O., Fink, C., Puderbach, M., Eichinger, M., Herth, F., Kauczor, H.U.: Assessment of the relationship between lung parenchymal destruction and impaired pulmonary perfusion on a lobar level in patients with emphysema. *European Journal of Radiology* **63** (2007) 76–83
13. Weinheimer, O., Achenbach, T., Bletz, C., Düber, C., Kauczor, H.U., Heussel, C.P.: About objective 3-d analysis of airway geometry in computerized tomography. *IEEE Trans. Med. Imaging* **27**(1) (2008) 64–74
14. Ley-Zaporozhan, J., Ley, S., Weinheimer, O., Iliyushenko, S., Erdugan, S., Eberhardt, R., Fuxa, A., Mews, J., Kauczor, H.U.: Quantitative analysis of emphysema in 3d using mdct: influence of different reconstruction algorithms. *Eur J Radiol* **65** (2008) 228–234
15. Heußel, C.P., Kappes, J., Hantusch, R., Hartlieb, S., Weinheimer, O., Kauczor, H.U., Eberhardt, R.: Contrast enhanced ct-scans are not comparable to non-enhanced scans in emphysema quantification. *European Journal of Radiology* **74**(3) (2010) 473–478
16. Brown, M.S., McNitt-Gray, M.F., Mankovich, N., Goldin, J.G., Hiller, J., Wilson, L.S., Aberle, D.R.: Method for segmenting chest ct image data using an anatomical model: Preliminary results. *IEEE Trans. Med. Imaging* **16**(6) (1997) 828–839
17. Brown, M.S., Goldin, J.G., McNitt-Gray, M.F., Greaser, L.E., Sapra, A., Li, K.T., Sayre, J.W., Martin, K., Aberle, D.R.: Knowledge-based segmentation of thoracic computed tomography images for assessment of split lung function. *Med Phys* **27** (Mar 2000) 592–598
18. Hu, S., Hoffman, E.A., Reinhardt, J.M.: Automatic lung segmentation for accurate quantitation of volumetric x-ray ct images - medical imaging, *ieee transactions on. IEEE TRANSACTIONS ON MEDICAL IMAGING* **20**(6) (2001) 490–498
19. Sluimer, I., Prokop, M., van Ginneken, B.: Toward automated segmentation of the pathological lung in ct. *IEEE TRANSACTIONS ON MEDICAL IMAGING* **24**(8) (2005) 1025–1038
20. Pu, J., Roos, J., Yi, C.A., Napel, S., Rubin, G.D., Paik, David S.: Adaptive border marching algorithm: Automatic lung segmentation on chest ct images. *Computerized Medical Imaging and Graphics* **32**(6) (2008) 452–462
21. Prasad, M.N., Brown, M.S., Ahmad, S., Abtin, F., Allen, J., da Costa, I., Kim, H.J., McNitt-Gray, M.F., Goldin, J.G.: Automatic segmentation of lung parenchyma in the presence of diseases based on curvature of ribs. *Academic radiology* **15**(9) (2008) 1173–1180
22. de Nunzio, G., Tommasi, E., Agrusti, A., Cataldo, R., de Mitri, I., Favetta, M., Maglio, S., Massafra, A., Quarta, M., Torsello, M., Zecca, I., Bellotti, R., Tangaro, S., Calvini, P., Camarlinghi, N., Falaschi, F., Cerello, P., Oliva, P.: Automatic lung segmentation in ct images with accurate handling of the hilar region. *Journal of digital imaging : the official journal of the Society for Computer Applications in Radiology* (2009)
23. Rikxoort, E.M., de Hoop, B., Viergever, M.A., Prokop, M., van Ginneken, B.: Automatic lung segmentation from thoracic computed tomography scans using a hybrid approach with error detection. *Med Phys* **36**(7) (2009) 2934–2947
24. Weinheimer, O., Achenbach, T., Düber, C.: Fully automated extraction of airways from ct scans based on self-adapting region growing. In Brown, M., de Bruijne,

- M., van Ginneken, B., Kiraly, A., Kuhnigk, J.M., Lorenz, C., McClelland, J., Mori, K., Reeves, A., Reinhardt, J., Reinhardt, J.M., eds.: Proceedings of the Second International Workshop on Pulmonary Image Analysis. (2009) 315–321
25. Gonzalez, R.C., Woods, R.E.: Digital image processing. 3. ed. edn. Pearson/Prentice Hall, Upper Saddle River, NJ (2008)
  26. Mueller, D., Maeder, A.: Robust semi-automated path extraction for visualising stenosis of the coronary arteries. *Computerized medical imaging and graphics : the official journal of the Computerized Medical Imaging Society* **32**(6) (2008) 463–475
  27. Mueller, D.: Fast marching minimal path extraction in itk. *The Insight Journal* (2008)